M. Nemec, H. Jelinkova, M. Miyagi, K. Iwai, and Y. Matsuura	250 μm inner diameter hollow waveguide for Er:YAG laser radiation	Proc. SPIE	Vol. 7173	71730H-1-71730H-8	2009
X. L. Tang, Y. W. Shi, Y. Matsuura, K. Iwai, and M. Miyagi	The effect of dielectric absorption on the transmission characteristics of terahertz hollow fibers	Proc. SPIE	Vol. 7173	71730N-1-71730N-9	2009
K. R. Sui, X. Lin, X. S. Zhu, Y. W. Shi, K. Iwai, and M. Miyagi	Fabrication of SiO_2/AgI/SiO_2/Ag hollow glass fiber for infrared transmission	Proc. SPIE	Vol. 7173	71730G-1-71730G-10	2009
T. Watanabe, K. Iwai, and Y. Matsuura	Simultaneous radiation of Er:YAG and Ho:YAG lasers for efficient ablation of hard tissues	Proc. SPIE	Vol. 7173	71730R-1-71730R-6	2009
K. Iwai, M. Miyagi, Y. W. Shi, X. S. Zhu, and Y. Matsuura	Fabrication of hollow optical fiber with a vitreous film for CO_2 laser light delivery	Proc. SPIE	Vol. 7173	71730Q-1-71730Q-7	2009
K. Iwai, A. Hongo, H. Takaku, M. Miyagi, J. Ishiyama, Y. W. Shi, and Y. Matsuura	Transmission properties of dielectric-coated hollow optical fibers based on silver-clad ding-stainless pipe	Proc. SPIE	Vol. 7559	755904-1-755904-12	2010
H. Jelinková, M. Nemec, P. Koranda, J. Pokorny, O. Kohler, M. Miyagi, K. Iwai, Y. Matsuura	Hollow waveguide for urology treatment	Proc. SPIE	Vol. 7559	755907-1-755907-7	2010
C. H. Yang, H. Hua, W. Tan, Y. W. Shi, K. Iwai, and M. Miyagi	FT-IR based loss-spectrum measuring system for infrared hollow waveguides	Proc. SPIE	Vol. 7559	75590R-1-75590R-8	2010
C. Yang, H. Hua, W. Tan, K. Iwai, M. Miyagi, N. Chi, and Y. Shi	Loss spectrum measurement for infrared hollow fiber based on the Fourier transform infrared spectrometer	Appl. Opt.	Vol. 49	2504-2509	2010

T. Watanabe, K. Iwai, T. Katagiri, and Y. Matsuura	Synchronous radiation with Er:YAG and Ho:YAG lasers for efficient ablation of hard tissues	Biomedical Optics Express	Vol. 1	337-346	2010

国内学会予稿集

発表者氏名	論文タイトル名	発表誌名	巻号	ページ	出版年
岩井 克全, 渡邊 智紀, 松浦 祐司	赤外レーザ光同時照射による軟組織の蒸散・凝固効果	平成20年度電気関係学会東北支部連合大会講演論文集		177	2008
岩井 克全, 宮城 光信, 石 芸尉, 松浦 祐司	赤外レーザ用内径100 μm中空ファイバの製作	電子情報通信学会通信ソサイエティ大会講演論文集		278	2008
渡邊 智紀, 岩井 克全, 松浦 祐司	Er:YAG, Ho:YAGレーザの同時照射による硬組織の高効率蒸散	電子情報通信学会通信ソサイエティ大会講演論文集		280	2008
岩井 克全, 宮城 光信, 石 芸尉, 朱 暁松, 松浦 祐司	CO_2レーザー光伝送用無機薄膜内装中空ファイバの製作	第29回レーザー学会学術講演会講演予稿集		220	2009
岩井 克全, 板垣 静香, 安藤 美帆, 宮城 光信, 石 芸尉, 松浦 祐司	赤外伝送用超細径銀中空ファイバの製作	電子情報通信学会総合大会講演論文集		490	2009
阿部 直雪, 庄子 健太郎, 岩井 克全, 宮城 光信, 石 芸尉	内径50 μm赤外伝送用銀中空ファイバの製作	平成21年度電気関係学会東北支部連合大会講演論文集		121	2009
岩井 克全, 高久 裕之, 宮城 光信, 石山 純一, 本郷 晃史, 石 芸尉	充填コーティング法を用いたAgI内装銀クラッドSUS管先端チップの製作	平成21年度電気関係学会東北支部連合大会		117	2009
岩井 克全, 高久 裕之, 宮城 光信, 石山 純一, 本郷 晃史, 石 芸尉	銀クラッドステンレス管を用いたAgI/Ag中空ファイバの伝送特性	電子情報通信学会通信ソサイエティ大会講演論文集		290	2009
岩井 克全, 本郷 晃史, 高久 裕之, 宮城 光信, 石山 純一, 石 芸尉	各種金属管を用いたCOP内装金属中空ファイバの伝送特性	レーザー学会学術講演会第30回年次大会講演予稿集		237	2010

岩井 克全, 本郷 晃史, 高久 裕之, 宮城 光信, 石山 純一, 石 芸尉	CO_2レーザ光伝送用極細金属プローブ	レーザー学会学術講演会第30回年次大会講演予稿集		237	2010
岩井 克全, 高久 裕之, 宮城 光信, 石山 純一, 本郷 晃史, 石 芸尉	AgI内装銀クラッドSUS中空ファイバのAgI膜厚制御	2010年電子情報通信学会総合大会講演論文集		532	2010
岩井 克全, 高久 裕之, 宮城 光信, 石 芸尉	中空ファイバにおける環状オレフィンポリマー成膜法の改善－COP溶液の濃度に対する粘度特性－	平成22年度電気関係学会東北支部連合大会講演論文集		69	2010
岩井 克全, 元木 沙綾, 宮城 光信, 石 芸尉	内径50 μm銀中空ファイバの伝送特性の改善	2010年電子情報通信学会エレクトロニクスソサイエティ大会講演論文集		159	2010
岩井 克全, 高久 裕之, 宮城 光信, 石 芸尉	無機薄膜内装高強度銀中空ファイバの製作	レーザー学会学術講演会第31回年次大会講演予稿集		241	2011

Method for evaluating material dispersion of dielectric film in the hollow fiber

Ke-Rong Sui,[1] Xiao-Song Zhu,[1,*] Xiao-Li Tang,[1] Katsumasa Iwai,[2] Mitsunobu Miyagi,[2,3] and Yi-Wei Shi[1]

[1]Department of Communication Science and Engineering, Fudan University, Shanghai 200433, China

[2]Sendai National College of Technology, Sendai, 989-3128, Japan

[3]Miyagi National College of Technology, Sendai, 981-1239, Japan

*Corresponding author: zhuxiaosong@fudan.edu.cn

Received 14 July 2008; revised 17 September 2008; accepted 24 October 2008; posted 31 October 2008 (Doc. ID 98810); published 21 November 2008

A method is proposed to evaluate the material dispersion of dielectric film in dielectric-coated silver hollow fiber. Cauchy's formulas that characterize the dispersion property were obtained for several commonly used dielectric materials by using the measured data of loss spectra of the hollow fibers. The wavelengths of the loss peaks and valleys in the loss spectra can be predicted more accurately when taking into consideration of the material dispersion. The derived Cauchy's formulas play an important role in the design of infrared hollow fiber for multiwavelength delivery. © 2008 Optical Society of America

OCIS codes: 060.2280, 230.7370, 310.6860, 260.2030.

1. Introduction

Dielectric-coated silver hollow fiber is one of the most commonly used infrared fibers in many applications [1–4]. It has low-loss property in the mid-infrared region, as well as in the visible and near-infrared (VIS-NIR) regions [5,6]. For a hollow fiber with a uniform and smooth dielectric inner-coating film, there are high-loss peaks and low-loss valleys in the loss spectra for the hollow fiber due to thin film interference. It is possible to use these low-loss valleys for multiwavelength delivery of infrared lasers and visible pilot beams. In the design and fabrication of high-performance hollow fiber, the low-loss valleys should be accurately located at the target wavelengths. By adjusting the film thickness of the dielectric layer, we can shift the wavelength of the low-loss valley to match the objective wavelength. However, theoretical calculation results do not agree well with the measured loss spectra because of the material dispersion of the dielectric film, especially in the VIS-NIR regions. Although optical constants for some of the dielectric materials can be found in the literature or published handbooks [7,8], they do not have data in the VIS-NIR regions or do not agree with the dispersion property of the dielectric film in the hollow fiber. This is because the film in the hollow fiber is formed by using unique fabrication techniques [9,10].

In this paper, we proposed a method to evaluate the dispersion property by using measured loss spectra of hollow fibers with various film thicknesses. Cauchy's formulas [11] for several commonly used materials were obtained. By taking into consideration the material dispersion, the wavelengths of the low-loss valleys in the VIS-NIR regions can be predicted more accurately. The derived Cauchy's formulas are of special importance to the design of high-performance infrared hollow fiber for multiwavelength laser light delivery.

2. Sample Preparation

Loss spectra of hollow fiber with various dielectric film thicknesses were needed in the evaluation for material dispersion. To prepare the samples, we used

0003-6935/08/346340-05$15.00/0

the chemical deposition method [6] to plate the silver layer on the inner surface of a glass capillary. Then the dielectric layer was coated upon the silver layer. The liquid-phase coating method was used for many dielectric materials, such as polymers [6,12] and silicone polymer [13]. Dielectric layers with different film thickness could be formed by modifying the concentration of the coating solution or the flowing speed in the fabrication process. For silver iodide (AgI) film, the iodination process [5] was used to turn the upper-side silver into AgI. The thickness of the AgI film could be controlled by changing iodination time, iodination temperature, or concentration of the iodination solution. For all of the hollow fiber samples made for the evaluation, the bore diameter is 0.7 mm and the length is around 25 cm.

3. Theoretical Evaluation

The loss spectrum of the dielectric-coated metallic hollow fiber has been theoretically evaluated [14,15]. For a hollow fiber of length z, the transmitted power $P(z)$ is

$$P(z) = \int_0^{\theta_{\max}} P_0(\theta) \exp\left[-\frac{1-R(\theta)}{2T\cot\theta} z\right] \sin\theta \mathrm{d}\theta, \qquad (1)$$

where $P_0(\theta)$ is the angular distribution of the incident beam, $R(\theta)$ is the power reflection coefficient, T is the inner radius of the hollow core, and $\theta_{\max}$ denotes the maximum launching angle. Theoretical result of loss spectrum for the hollow fiber was obtained by calculating $P(z)$ in a certain wavelength region. Because the power reflection coefficient $R(\theta)$ is dependent on the refractive index of the dielectric film, material dispersion has a great influence on the position of low-loss valleys in the loss spectra.

There are normally obvious interference peaks in the measured loss spectra of the hollow fiber when a uniform and smooth inner dielectric film is formed. These peaks at various wavelengths, along with the film thickness, contain information on the dispersion property of the dielectric film. We use Cauchy's formula $n(\lambda) = A + B/\lambda^2 + C/\lambda^4$ [11] to evaluate the dispersion. In order to calculate the constants A, B, and C in Cauchy's formula, we need the measured loss spectra of the hollow fiber with different film thicknesses. Loss spectra in the VIS-NIR regions were measured for samples prepared as described in Section 2. Figure 1 is the schematic setup for measuring the loss spectrum of the hollow fiber in the VIS-NIR regions. An incoherent white light was used as the light source, and it was coupled into the hollow fiber through a GI fiber with 600 μm core diameter. The light at the output end was received by the spectrum analyzer (Advantest Q8344A). Loss spectra of the hollow fiber were obtained by comparing the output light with the input light as the background.

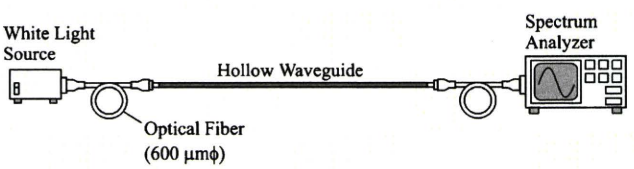

Fig. 1. Schematic setup for loss spectrum measurement.

Due to the difference of film thicknesses among samples, loss peaks, and valleys appeared at various wavelengths in their loss spectra. For each loss spectrum, we define λ_m as the mth wavelength from longer to shorter wavelength at which loss peak appears. Also, $n_i(\lambda_m)$ is defined as the refractive index at the wavelength of λ_m in the ith loss spectrum. The order of the loss spectra was arranged randomly. Here we take AgI material as an example to show the evaluation method for Cauchy's formula in VIS-NIR regions.

1. $n_1(\lambda_1)$, the refractive index of AgI at the wavelength of λ_1 in the first loss spectrum, is taken from the literature [8] as the initial value in the calculation circles.
2. Make λ_1 in the theoretical loss spectrum agree with the λ_1 in the measured loss spectrum by adjusting the film thickness, and we get a film thickness d.
3. By using the thickness d in step (2), make λ_2 in the theoretical loss spectrum agree with the λ_2 in the measured loss spectrum by adjusting the refractive index at the wavelength λ_2. Then we get $n_1(\lambda_2)$.
4. Do step (3) to other $\lambda_m(\lambda_3, \lambda_4 \ldots)$, and we get the refractive indices of AgI at the wavelengths of all the peaks in this measured loss spectrum, $n_1(\lambda_m)$.
5. Repeat steps (1) to (4) for all the measured loss spectra. Record the data of $n_i(\lambda_m)$ of every loss spectrum and put them together, then we get a group of refractive index–wavelength data $n_i(\lambda_m)$ for the AgI material ($i = 1, 2, 3, \ldots$, $m = 1, 2, 3, \ldots$).
6. Use Cauchy's formula $n(\lambda) = A + B/\lambda^2 + C/\lambda^4$ as the formula to fit the data of refractive indices in step (5), and we get an empirical formula of material dispersion for the AgI film.
7. New $n_i(\lambda_m)$ are calculated by the empirical formula for every measured loss spectrum and it is used in step (1) in the next calculation cycle instead of the initial one.
8. Repeat steps (1) to (7) and new formulas are gotten in every cycle. Stop the process when the difference between film thicknesses d in two continuous circles is smaller than 1% for all the measured loss spectra.

Finally, an empirical formula of material dispersion for the AgI film in the AgI/Ag hollow fiber is derived.

As a consequence of the fabrication techniques [16], the thickness of the dielectric film can be tapered along the length of fiber. The tapered thickness will widen the interference peaks in the loss spectra and the position of the peaks should be determined by the average thickness. The thickness d in the evaluation method refers to the average thickness of the dielectric film, and therefore the slightly tapered film does not affect the evaluation method. Moreover,

because the fiber samples fabricated for the evaluation were of short length, we can neglect the variation of film thickness along the fiber.

4. Results

We have applied this method to four kinds of commonly used dielectric materials in the hollow fiber. They are cyclic olefin polymer (COP) [6], silicone polymer (R_2SiO) [12], Arton polymer [13], and AgI [5]. The empirical formulas of their dispersion properties have been calculated. The constants A, B, and C in the empirical formula for the four kinds of material are summarized in Table 1, where λ is in micrometers. In our recent paper [17], the empirical formula of AgI proved that it is helpful for accurately predicting the transmission properties of the hollow fiber in the VIS-NIR regions.

Figure 2 shows the refractive indices of AgI and R_2SiO in the VIS-NIR regions. Curves 1 and 3 (dashed lines with data dots) are data of AgI and silicon dioxide (SiO_2) in the literature [8]. Curves 2 and 4 (solid lines) are results obtained by using the empirical formula in Section 3. Normally, the optical constants in the literature were obtained by measuring the optical properties of bulk material. Thin film has different optical properties from that of the bulk material. This is because bulk material and thin film are made by using different fabrication processes, and the crystalline phase of the material may not be the same, e.g., AgI [18]. Moreover, the R_2SiO film formed by using silicone polymer was a vitreous layer that was similar to but not pure SiO_2. This might be the reason for the large difference between curves 3 and 4. Figure 3 shows the refractive indices of COP and Arton calculated by the empirical formula. We have not found any other dispersion data about COP and Arton for comparison.

It can be seen in Figs. 2 and 3 that the refractive indices of the four kinds of material change more rapidly in the visible region. Therefore in the loss spectra of the hollow fiber, the intervals between adjacent peaks in visible region are much smaller than that in the infrared region. We should pay more attention to the dispersion property of the dielectric film in the VIS-NIR regions when designing an infrared hollow fiber for simultaneous delivery of a visible laser light. In addition, if the dielectric material has no resonance absorptions in the mid-infrared region, this method can also be applied to the evaluation for the dispersion property of the dielectric film in the mid-infrared regions.

Table 1. Constants in Cauchy's formula for Four Kinds of Dielectric Film Materials in Hollow Fiber

Material	A	B	C
COP	1.50815	0.01653	−0.00026
R_2SiO	1.42614	0.02729	0.0001
Arton	1. 52743	0.01855	0.00028
AgI	2.0216	0.0878	−0.0024

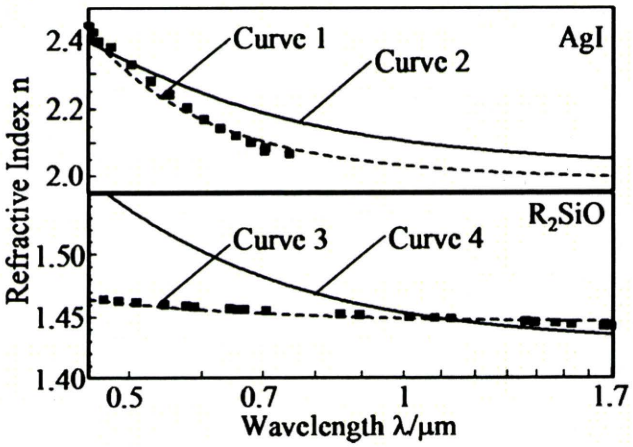

Fig. 2. Refractive indices of AgI and R_2SiO in the VIS-NIR regions. The dashed lines with data dots are from the data published in the literature [8].

Figure 4 is the loss spectra of the R_2SiO-coated silver (R_2SiO/Ag) hollow fiber. The fiber was of 0.7 mm bore size and 1 m length. Calculated 1 corresponds to the theoretical result considering material dispersion from the empirical formula (i.e., curve 4 in Fig. 2). Calculated 2 corresponds to the result considering material dispersion from the literature [8] (i.e., curve 3 in Fig. 2), and calculated 3 corresponds to the result without considering material dispersion. It can be seen that calculated 1 agrees well with the measured result. Calculated 2 and 3 did not agree with the measured result especially in the visible wavelength region. The disagreement may cause mistakes in structure design for the hollow fiber. That is, the loss valley will be arranged at the wrong wavelength when we neglect the material dispersion or take inappropriate data about the material dispersion.

Figure 5 shows the measured loss spectra of R_2SiO/Ag, Arton-coated silver (Arton/Ag), COP-coated silver (COP/Ag), and AgI/Ag hollow fibers. Fibers are 1 m long and 0.7 mm in diameter. None of these measured spectra was used in the calculation

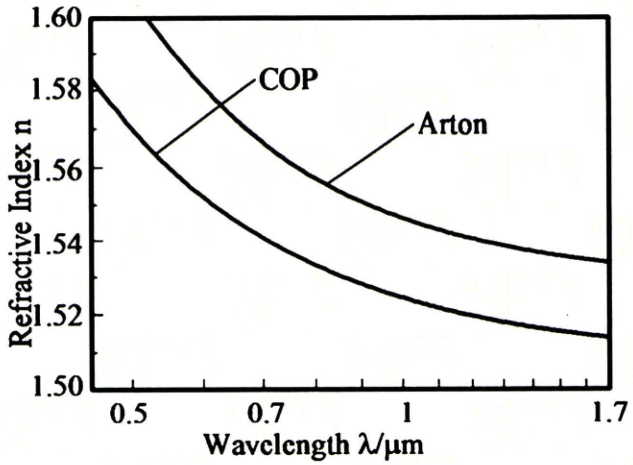

Fig. 3. Refractive indices of COP and Arton polymer in the VIS-NIR regions.

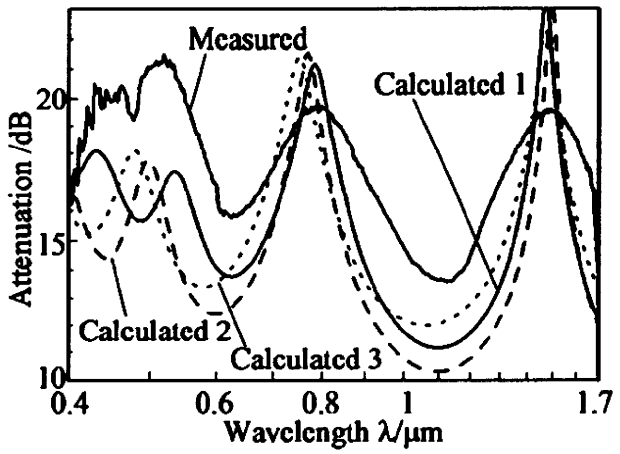

Fig. 4. Theoretical loss spectra of R_2SiO/Ag hollow fiber calculated by using different material dispersion formulas. Measured loss spectrum is also shown for comparison.

in Section 3 for deriving Cauchy's formula. Theoretical loss spectra considering material dispersion from the empirical formulas are also included. In the calculation the absorption of material was neglected, because the absorption in the VIS-NIR regions is very small, normally smaller than 10^{-3} [19]. There is a discrepancy in loss values between measurements and calculations in Fig. 5. Absorption of the material is one reason for the discrepancy. Another reason is the nonuniformity of the dielectric film thickness, which causes additional loss. Moreover, the surface roughness was set to be a certain value in the calculation. This may also cause a discrepancy in the loss magnitude. The results in this paper are qualitatively rather than quantitatively correct, which is due to the approximate nature of the Cauchy's formula and the above-mentioned reasons. But the formula is supposed to be used for predicting the positions of loss valleys, which are most important in the structure design for high-performance hollow fibers. And good agreement between valley positions shows that it works rather well when taking into consideration the derived dispersion. That is, the derived Cauchy's formula characterized the dispersion property of the dielectric film in the hollow fiber well.

5. Conclusions

Material dispersion plays an important role in the design of high-performance dielectric-coated metal hollow fiber. For most of the commonly used dielectric film materials in the hollow fiber, there are few data about the dispersion property in the VIS-NIR regions. And some data found in handbooks do not agree with the dispersion property of the film due to different fabrication techniques. We proposed a method to evaluate the material dispersion of the dielectric film in the hollow fiber. Empirical formulas for four kinds of dielectric film materials were derived according to Cauchy's formula of material

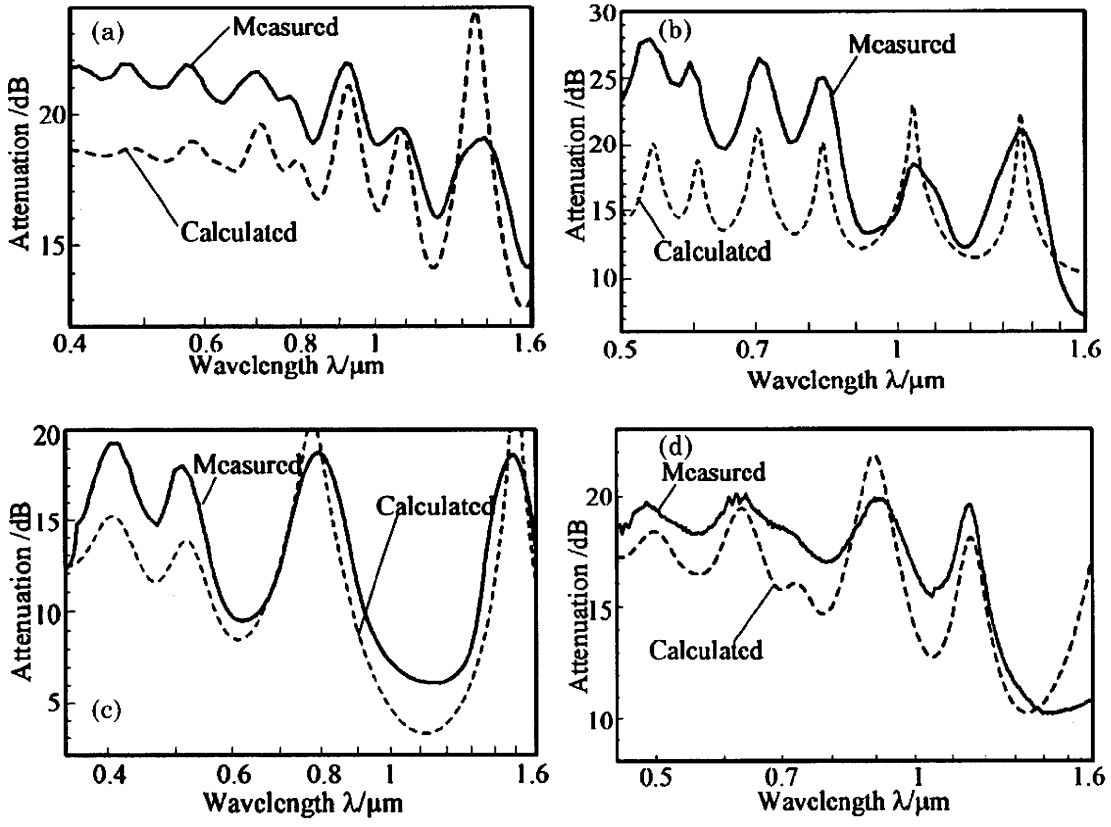

Fig. 5. Theoretical and measured loss spectra of the dielectric-coated silver hollow fibers. (a) R_2SiO, (b) Arton/Ag, (c) COP/Ag, and (d) AgI/Ag hollow fiber.

dispersion. By taking into consideration of the material dispersion with these formulas, the wavelengths of the low-loss valleys in the VIS-NIR regions can be predicted more accurately in the structure design for the hollow fiber. These formulas provide an important role for the design of high performance dielectric-coated silver hollow fiber. The basic thought of this method may also be helpful in other optical experiments for deriving optical constants from experimental measured data.

This work is financially supported by the National Nature Science Foundation of China (NSFC, 60608013), the Shanghai Pujiang program (7pj14012), and the Ministry of Education, Science, Sports and Culture of Japanthrough Grant-in-Aids for Scientific Research (B) (20360164).

References

1. V. Gopal, J. A. Harrington, A. Goren, and I. Gannot, "Coherent hollow-core waveguide bundles for infrared imaging," Opt. Eng. **43**, 1195–1199 (2004).
2. S. Sato, Y. W. Shi, Y. Matsuura, M. Miyagi, and H. Ashida, "Hollow-waveguide-based nanosecond, near-infrared pulsed laser ablation of tissue," Lasers Surg. Med. **37**, 149–154 (2005).
3. J. Raif, M. Valid, O. Nahlieli, and I. Gannot, "An Er:YAG laser endoscopic fiber delivery system for lithotripsy of salivary stones," Lasers Surg. Med. **38**, 580–587 (2006).
4. H. Jelinkova, T. Dostalova, M. Nemec, P. Koranda, M. Miyagi, K. Iwai, Y. W. Shi, and Y. Matsuura, "Free-running and Q-switched Er:YAG laser dental cavity and composite resin restoration," Laser Phys. Lett. **4**, 835–839 (2007).
5. R. George and J. A. Harrington, "Infrared transmissive, hollow plastic waveguides with inner Ag-AgI coatings," Appl. Opt. **44**, 6449–6455 (2005).
6. Y. W. Shi, K. Ito, L. Ma, T. Yoshida, Y. Matsuura, and M. Miyagi, "Fabrication of a polymer-coated silver hollow optical fiber with high performance," Appl. Opt. **45**, 6736–6740 (2006).
7. Y. Wang, Y. Abe, Y. Matsuura, M. Miyagi, and H. Uyama, "Refractive indices and extinction coefficients of polymers for the mid-infrared region," Appl. Opt. **37**, 7091–7095 (1998).
8. E. D. Palik, *Handbook of Optical Constants of Solids* (Academic, 1985).
9. Y. Matsuura, T. Abel, and J. A. Harrington, "Optical properties of small-bore hollow glass waveguides," Appl. Opt. **34**, 6842–6847 (1995).
10. Y. Kato, M. Osawa, M. Miyagi, M. Aizawa, S. Abe, and S. Onodera, "New fabrication technique of fluorocarbon polymer-coated hollow waveguides by liquid-phase coating for medical applications," Proc. SPIE **2131**, 4–10 (1994).
11. M. Born and E. Wolf, *Principles of Optics*, 7th ed. (Cambridge U. Press, 1999).
12. S. Ouyang, Y. W. Shi, Y. Matsuura, and M. Miyagi, "Rugged distal tips for CO_2 laser medicine," Opt. Laser Technol. **35**, 65–68 (2003).
13. K. Iwai, M. Miyagi, Y. W. Shi, X. S. Zhu, and Y. Matsuura, "Infrared hollow fiber with a vitreous film as the dielectric inner coating layer," Opt. Lett. **32**, 3420–3422 (2007).
14. Y. Matsuura, M. Saito, M. Miyagi, and A. Hongo, "Loss characteristics of circular hollow waveguides for incoherent infrared light," J. Opt. Soc. Am. A **6**, 423–427 (1989).
15. M. Miyagi and S. Kawakami, "Design theory of dielectric-coated circular metallic waveguides for infrared transmission," J. Lightwave Technol. **2**, 116–126 (1984).
16. K. Iwai, Y. W. Shi, M. Miyagi, and Y. Matsuura, "Improved coating method for uniform polymer layer in infrared hollow fiber," Opt. Laser Technol. **39**, 1528–1531 (2007).
17. K. R. Sui, Y. W. Shi, X. L. Tang, X. S. Zhu, K. Iwai, and M. Miyagi, "Optical properties of AgI/Ag hollow fiber in the visible wavelength region," Opt. Lett. **33**, 318–320 (2008).
18. R. Dahan, J. Dror, and N. Croitoru, "Characterization of chemically formed silver iodide layers for hollow infrared guides," Mater. Res. Bull. **27**, 761–766 (1992).
19. Y. Wang and M. Miyagi, "Simultaneous measurement of optical constants of dispersive material at visible and infrared wavelengths," Appl. Opt. **36**, 877–884 (1997).

Dual-wavelength laser irradiation through hollow optical fiber for hard tissue ablation

Tomonori WATANABE [1)], Katsumasa IWAI [2)], and Yuji MATSUURA [1)]

1) Tohoku University, Department of Electrical Communications, Sendai 980-8579, Japan
2) Sendai National College of Technology, Sendai 989-3128, Japan

Abstract

Laser ablation experiments on hard tissues are performed by guiding combined beam of Ho:YAG and Er:YAG laser light with a hollow optical fiber. An alumina ball is used as a hard-tissue model and ablation phenomenon are observed by an ultra-high-speed camera. The result show that the two laser light give dissimilar ablation effects due to different absorption coefficients in water contained in the tissues. When the two lasers are combined and irradiate on the model, a high ablation rate is observed.

Keywords: Laser treatment, Hard tissue ablation, Infrared lasers, Hollow optical fibers

1. Introduction

Since bio-tissues contains water that strongly absorbs infrared light, irradiation by infrared light has a large effect on both of hard and soft tissues and therefore, it is applied to variety of medical applications[1]. Low invasive therapies using a laser endoscope have been developed to radiate laser light inside human body by using an optical fiber incorporated in the endoscope. These laser endoscopes are getting popular in urological applications such as ablation of the prostate and fragmentation of urinary calculi and usually, Nd:YAG lasers with the wavelength of 1.06 μm or Ho:YAG lasers of 2.1 μm is used because a common silica-glass fiberoptics can be employed as delivery medium of laser light[2]. Recently an Er:YAG laser with the 2.94-μm wavelength is reportedly more effective for calculus fragmentation[3] because the laser light is strongly absorbed with calcium oxalate and magnesium ammonium phosphate contained in urinary calculi[4].

Er:YAG lasers have, however, a drawback that a flexible silica-glass fiber cannot be used for laser delivery because of the absorption losses at the relatively long wavelength of 2.94 μm. Our group have proposed and developed a hollow optical fiber for Er:YAG laser delivery. Hollow optical fibers have no absorption loss in the airy core and show highly efficient transmission for any wavelengths in the infrared. Because the hollow optical fibers also have high durability for laser radiation, they are already employed as a flexible transmission line in laser treatment systems in the market.

Optical Fibers and Sensors for Medical Diagnostics and Treatment Applications VIII,
edited by Israel Gannot, Proc. of SPIE Vol. 6852, 68520E, (2008) · 1605-7422/08/$18
doi: 10.1117/12.761421

In this paper, we investigate effects of simultaneous irradiation by Ho:YAG and Er:YAG lasers on hard tissues such as calculi and teeth. Although there have been some reports on irradiation of lasers with different wavelengths for medical applications, they usually are for incision and ablation of soft tissues where both of high incision rate and hemostatic effect are required[5]. Here we investigate ablation mechanisms of the lasers to achieve higher ablation effect for hard tissues.

2. Experiment and Discussion

We used an experimental setup shown in Fig. 1 to irradiate a hard tissue model with the two different lasers light. Ho:YAG and Er:YAG laser light are combined by using a dichroic mirror and the laser beam is focused by a f=76 mm CaF_2 lens on the input end of a short hollow-fiber tip (100 mm in length) employed as a coupling optics. A hollow optical fiber with an inner diameter of 0.7 mm is butt-coupled to the short fiber that has the same diameter. The hollow fiber is coated with silver and cyclic-olefin polymer (COP) thin film on the inside[6] and the thickness of COP is 0.3 μm so that the transmission losses for both of Er:YAG and Ho:YAG lasers are reduced by interference effect of the polymer film that acts as a reflection enhancement coating. The transmission losses of the hollow optical fiber used in the experiment are 1.0 dB for Ho:YAG and 0.5 dB for Er:YAG laser light.

The distal end of the hollow optical fiber is capped to keep the inside of fiber from vapor and debris of the ablated tissues. We proposed, for hollow optical fibers, glass lens caps that offer a high ablation efficiency owing the higher energy intensity of focused beam[7]. In the experiment, we used two kinds of caps that are, as shown in Fig. 2, a ball-lens cap and a hemispherical lens cap. The focusing effect of the caps is shown in Fig. 3 as changes of measured beam sizes in distance from the lens surface. The result show that focal lengths of the caps are 1.0 mm for the hemispherical and 0.1 mm for the ball lens caps. The insertion loss of the cap is around 15% and therefore, the energy density at the focused spot is around twice of the unfocused beam.

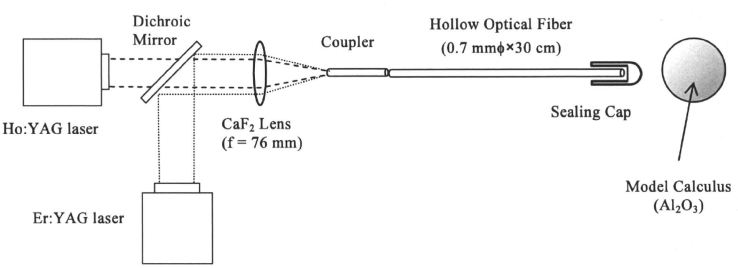

Fig. 1 Experiment setup for dual-wavelength irradiation

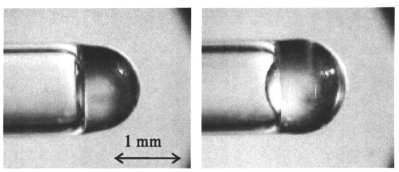

(a) Hemisphere (b) Ball

Fig. 2 Focusing glass caps for hollow optical fibers

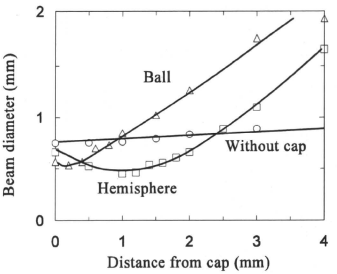

Fig. 3 Beam diameter in distance from cap surface

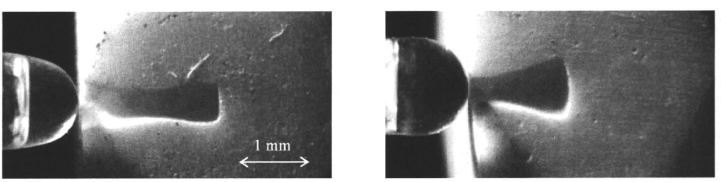

(a) Using hemisphere cap (b) Using ball lens cap

Fig. 4 Cutting sections of ceramic balls after irradiated with Er:YAG laser pulses

To test the ablation capability of the lens caps, Er:YAG laser light irradiates alumina ceramic balls used as a hard tissue model. The balls are 4-7 mm in diameter and immersed in water before the test so that the balls contain water in high volume. Figure 4 shows cutting sections of the balls after irradiated with 10 Er:YAG-laser pulses of 300 μs in pulse width, 10 Hz in frequency, and 100 mJ in pulse energy. The result shows that ablation depth is around 40% larger in the one employed the hemisphere cap and this is because of the smaller divergence angle from the cap. From this result, we used the hemisphere cap in the experiments hereafter.

We firstly compared ablation capabilities of Ho:YAG and Er:YAG laser light for hard tissues by evaluation of depth and width of ablated holes as a function of number of laser pulses. Pulse energy used in the test was 100 mJ at repetition rate of 10 Hz and the pulse widths are 250 μs for Ho:YAG and 300 μs for Er:YAG lasers. As seen from the result in Fig. 5, the widths are comparable for the both lasers and, in contrast, the result on the depth shows different appearances for the two lasers. When irradiated with Er:YAG laser light, the depth linearly increases with the number of pulses. For the Ho:YAG, however, it is saturated with number of pulses. This is because energy density of the laser beam falls the ablation threshold of hard tissues when the beam

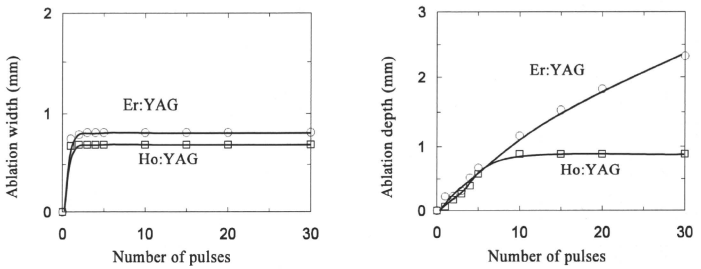

Fig. 5 Depth and width of ablated holes as a function of number of laser pulses

spreads due to focusing effect of the lens cap. This happens in lower energy density for the Ho:YAG laser because of the lower absorption coefficient in water.

Secondly we observed ablation phenomenon by using an ultra-high-speed camera to investigate difference in the ablation mechanisms of the two lasers. Figure 6 shows a moment of ablation with laser pulse energy of 100 mJ recorded at 50,000 frame/sec of capture speed. When irradiated with Er:YAG laser light, powdery dust are scattered from the surface immediately after laser radiation. This is because the laser energy is absorbed in very surface of the tissue. On the other hand, for the Ho:YAG laser, relatively large debris are spattered after the surface swelled. The laser beam penetrates into the tissue and an explosive ablation occurred from the inside. From these results, we expect, owing to the different ablation mechanisms, a high ablation effect when properly combining the two lasers beams.

In the next experiment, the two laser beams are combined and shoot an alumina ball to investigate effects of simultaneous irradiation. The pulse energies are 200 mJ for Ho:YAG and 100 mJ for Er:YAG laser,

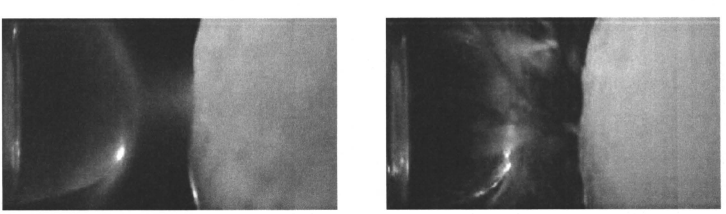

(a) Er:YAG (b) Ho:YAG

Fig. 6 Moment of ablation with Er:YAG and Ho:YAG laser pulse

and the repetition rates are 10 Hz for the both lasers. Figure 7 shows measured quantities of ablation when the two lasers irradiate the sample simultaneously and independently. The result "independent" is the sum of the ablation weight for the two lasers that were separately measured. The ablation quantities linearly increase with number of laser pulses and we found that the ablation efficiency is around 20% higher in the simultaneous irradiation. Figure 8 shows cutting sections of alumina balls ablated with Ho:YAG and Er:YAG lasers. With the Er:YAG laser light, the ablation proceeds to depth direction and the stress of the ablation brings destruction of the surface. For the Ho:YAG laser, in contrast, ablation uniformly occurs in lateral direction. When these two lasers irradiate the tissue simultaneously, the ablation occurs in both of depth and lateral directions and, as a result, the high ablation capability is obtained.

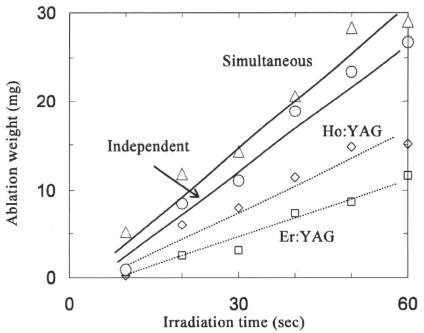

Fig. 7 Ablation weight after irradiated with two lasers simultaneously and independently

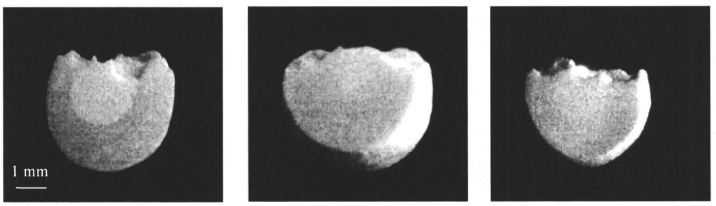

(a) Er:YAG (b) Ho:YAG (c) Er:YAG + Ho:YAG

Fig. 8 Cutting section of alumina balls ablated with Er:YAG and Ho:YAG lasers

3. Conclusion

Laser ablation experiments on hard tissues are performed by guiding combined beam of Ho:YAG and Er:YAG laser light with a hollow optical fiber. An alumina ball is used as a hard-tissue model and ablation phenomenon are observed by an ultra-high-speed camera. The result show that the two laser light give dissimilar ablation effects due to different absorption coefficient in water contained in the tissues. When the two lasers are combined and irradiate on the model, a high ablation rate is observed. In the experiments shown in this paper, the pulses of the two different lasers are not synchronized. Much higher effect of simultaneous irradiation is expected if they are synchronized and the pulse timing is finely tuned to maximize the effect. The experiment is carried on in our group and the result will be reported elsewhere.

References

1. A. Aoki, et al., "Comparison between Er:YAG laser and Conventional Technique for Root Caries Treatment in vitro," J. Dent. Res., **77**, 1404-1414 (1998)
2. M. K. Yiu, et al., "Clinical Experience With Holmium:YAG Laser Lithotripsy of Ureteral Calculi," Lasers Surg. Med., **19**, 103-106 (1996)
3. H. Lee, et al., "Urinary calculus fragmentation during Ho:YAG and Er:YAG lithotripsy," Lasers Surg. Med., **38**, 39-51 (2006)
4. K. F. Chan, et al., "Free Electron Laser Ablation of Calculi: An Experimental Study," IEEE J. Quantum Electron., **7**, 1022-1033 (2001)
5. T. Amagai, et al., "An Experimental Pathologic Study of Gingivectomy Using Dual-Wavelength Laser Equipment With OPO," Lasers Surg. Med., **39**, 51-58 (2007)
6. M. Miyagi, et al., "Design theory of dielectric-coated circular metallic waveguides for infrared transmission," J. Lightwave Technol., **LT-2**, 116-126 (1984)
7. K. Iwai, et al., "Erbium:YAG laser lithotripsy by use of a flexible hollow waveguide with an end-scaling cap," Appl. Opt., **42**, 2431-2435 (2003)

Thin Hollow Glass Waveguide for Near IR Radiation Delivery

Michal Němec[a*], Helena Jelínková[a], Jan Šulc[a]
Mitsunobu Miyagi[b], Katsumasa Iwai[b],Yi-Wei Shi[c], Yuji Matsuura[d]
[a]Faculty of Nuclear Sciences and Physical Engineering
Czech Technical University, Břehová 7, 115 19 Prague 1, Czech Republic
[b]Sendai National College of Technology, Aoba-ku, Sendai, 989-3128, Japan
[c]School of Information Science and Engineering, Fudan University, Shanghai, 200433, China
[d]Graduate School of Engineering, Tohoku University, Sendai 980-8579, Japan

ABSTRACT

The delivery of the radiation by thin fiber is required for some application, especially in medical internals treatment. Therefore a new 100 μm and 250 μm inner diameter hollow glass waveguides were developed and investigated for the possibility to transport high power near infrared laser radiation without damage of these delivery systems. As laser sources two Nd:YAG laser systems working in Q-switched regime at wavelength 1.06 μm and 1.34 μm were utilized. Delivered radiation characterization was performed. By Alexandrite laser (755 nm) pumped Q-switched Nd:YAG laser has been generating 1.06 μm wavelength radiation with 6 ns length of pulse and maximum output energy 0.7 mJ (116.7 kW). The laser was Q-switched using $LiF:F^{2-}$ saturable absorber. Second laser system was Nd:YAG/V:YAG microchip pumped by laser diode operating at 808 nm. The radiation at 1.3 μm wavelength has been generated with 250 Hz repetition rate. Pulse length was 6 ns and mean output power 25 mW. Corresponding pulse energy and peak power was 0.1 mJ and 16.7 kW, respectively. Both lasers were operating in fundamental TEM_{00} mode ($M^2 \sim 1$). For delivery a special cyclic olefin polymer-coated silver hollow glass waveguides with the inner/outer diameters 100/190 μm and 250/360 μm were used. The delivery system was consisted of lens, protector, and waveguide. As results the transmission more than 55 % and reasonable spatial profile of laser output radiation were found. From these measurements it can be recommended using of this system for near infrared powerful radiation delivery as well as for medical treatment.

Keywords: Hollow glass waveguide, IR lasers, spatial structure.

1. INTRODUCTION

Detailed knowledge of interaction beam spatial structure can be lead to precise laser applications in the medicine, industry, and also their use in research laboratories. Generally an articulated arm, optical fiber, and hollow waveguide are used as delivery systems of laser beam. Poor manipulability of the articulated arms reduces their utilization[1]. And for high power pulses, the third delivery type appears the best due to air core, high power damage threshold, low insertion losses, no end reflection, so we focused to hollow glass waveguides.

New waveguide types are investigated and better transfer properties of hollow waveguides are still developed[2-4]. The interaction beam spatial structure is another significant parameter and together with dimension of waveguides can define final application. So for ophthalmology, urology, dentistry or micro-surgery, the delivery of the radiation by thin waveguide is requested.

In the last year, we reported delivered systems with waveguide diameter of 700/850 μm[5]. The modification of the beam spatial structure during the propagation through the waveguide (cyclic olefin polymer coated silver hollow glass waveguide) was investigated for near and mid infrared radiation – 1.98 μm, 2.01 μm and 2.94 μm wavelength. The defined beam profile (approximately Gaussian mode) from the laser systems was changed into many peak structures having dominant intensity in the center.

* michal.nemec@fjfi.cvut.cz; phone +420 224 358 672; fax +420 222 512 735;

Optical Fibers and Sensors for Medical Diagnostics and Treatment Applications VIII,
edited by Israel Gannot, Proc. of SPIE Vol. 6852, 68520W, (2008) · 1605-7422/08/$18
doi: 10.1117/12.761837

The aim of the this work was to investigate the delivery high peak power near-infrared radiation (1.06 μm and 1.34 μm wavelength) by 100/190 μm and 250/360 μm thin hollow glass waveguides and the modification of the beam spatial profile, as well as the possibility of its utilization in medical application.

2. MATERIALS AND METHODS

2.1. Laser sources

2.1.1. Alexandrite laser radiation pumped Nd:YAG laser

The first Nd:YAG laser, operating at wavelength 1.06 μm, was coherently pumped by Alexandrite laser (755 nm emission wavelength, 30 mJ output energy, pulse duration 50 μs). As a laser active medium 60 mm long Nd:YAG rod was used (1 at.% Nd/Y, diameter 5 mm, AR/AR-coated faces). The pumping beam was focused into this crystal by a lens with 150 mm focal length. The crystal was placed into the 110 mm long linear resonator. The semihemispherical laser cavity was formed by a pumping spherical mirror and by flat output coupler. The pumping mirror (radius r = 500 mm) had high transmittance at the pumping (740–750 nm) wavelength and maximal reflectance at the oscillating wavelength about 1 μm. The output coupler reflectance was 60 % @ 1064 nm. Neodymium laser was Q-switched using $LiF:F_2^-$ saturable absorber ($T_0 \sim 70$ %) which was placed inside the resonator between Nd:YAG rod and the output coupler. This configuration allows us to obtain stable well reproducible short powerful giant pulses.

Laser repetition rate of 5 Hz was done by repetition rate of Alexandrite laser power supply. The maximum output energy (peak power) and pulse length were 0.7 mJ (116.7 kW) and 6 ns, respectively. Laser was operating in a fundamental TEM_{00} mode ($M^2 \sim 1$). Generated radiation was unpolarized.

2.1.2. Diode pumped Nd:YAG/V:YAG laser

The second laser system was based on diode pumped Nd:YAG/V:YAG laser microchip, operating at wavelength 1338 nm[6]. This laser used specially developed sandwich crystal which combined in one piece the cooling undoped part (undoped YAG crystal 4 mm long), the active laser part (YAG crystal doped with Nd^{3+} ions, c = 1.1 % Nd/Y, 12 mm long), and the saturable absorber (YAG crystal doped with V^{3+} ions 0.7 mm long). The diameter of this crystal was 5 mm. The microchip resonator consisted of dielectric mirrors which were deposited directly on the monolith crystal surfaces. The pump mirror with the high transmission for pump radiation and the high reflection for generated radiation was placed on the undoped YAG part. The output coupler with reflectivity 90 % for the generated wavelength was placed on the V^{3+}-doped part. The total microchip laser resonator length was 16.7 mm. For this laser pumping a laser diode HLU20F400 (LIMO Laser Systems) was used. The diode was emitting radiation at wavelength 808 nm with the maximum output power 20 W at the end of the fiber (fiber core diameter: 400 μm; numerical aperture: 0.22). This radiation was focused into the active Nd:YAG crystal by two achromatic doublet lenses (focal length f = 75 mm). The laser diode was operating in pulsed regime (rep. rate 250 Hz, pulse width 300 μs, pulse energy 6 mJ) with duty-factor 7.5 % to reduce thermal effects inside the microchip laser.

Using this laser, stable and high reproducible Q-switched pulses were generated at wavelength 1338 nm. Pulse length was 6 ns (FWHM). The output mean power was 25 mW which corresponds to single pulse energy and peak power 0.1 mJ and 16.7 kW, respectively. The laser was operating in the fundamental TEM_{00} mode ($M^2 \cong 1$).

2.2. Delivery system – hollow glass waveguide

In this work, a polymer coated silver hollow glass waveguides were utilized as the delivery system. The waveguides consist of a fused silica glass tube coated inside with silver layer covered by a dielectric layer. This layer enhances the reflectance of transmitted light on the inner surface of the waveguide. As dielectric coating material, a cyclic olefin polymer (COP) was chosen. The thickness of dielectric film can be realized from 0.1 μm depending on the transmitted wavelength of radiation. The COP silver hollow glass waveguides were successfully produced with the length up to 2 m and with 1 mm, 700 μm, 540 μm, and 320 μm inner diameters. A polyimide protective layer was used on the fused silica tube outside surface. The mechanical strength of the waveguides was determined by the silica glass tubing.

New manufactured samples (investigated in this work) had the inner diameters 100 μm and 250 μm, and the outer diameters 190 μm and 360 μm, respectively. The length of trial samples was 10 cm. At disposal it was one 100 μm (1A6-11-2) and four 250 μm (C25-3-0, C25-3-1, C25-3-2, C25-3-4) waveguides. A very good flexibility done by thin silica glass tube was proved for this waveguide types (Fig.1).

For a protection of the waveguide input face and input inner layers during the adjustment stage of the system, a special tube-shaped protector was inserted at the beginning of the delivery system.

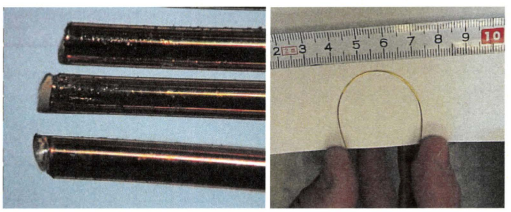

Fig. 1. Photo of COP coated silver hollow glass waveguides with the 250/360 μm diameter.

2.3 Measuring instruments and methods

The characterization was performed for both – the radiation entering into the waveguide, and the delivered one. The laser radiation energy, time dependence, and the spatial structure were measured. For measurement of the energy the two-channel Molectron JD 2000 Joulemeter/Ratiometer with Molectron probes (model No. J25) was used. The waveform was investigated by PIN detector ET-3000 (InGaAs, EOT) connected with the Tektronix 3052B scope. The radiation power was measured by Molectron EPM 2000 power meter with Molectron PM3 probe. The beam spatial structure was monitored by the Electrim CCD camera (EDC-1000HR) or pyroelectric camera (Spiricon Pyrocam III).

Due to the very high stability of the generated laser radiation, the transmission of the waveguide system was calculated from consecutively performed measurement of the input and output energy before and behind the waveguide.

3. RESULTS

3.1 Delivery of 1.06 μm Nd:YAG laser radiation

The Nd:YAG laser radiation coherently pumped by the Alexandrite laser generated the fundamental TEM_{00} mode with $M^2 \cong 1$ (Fig.2). The maximum output energy was 0.7 mJ in the pulse with length of 6 ns, the corresponding power was 116.7 kW.

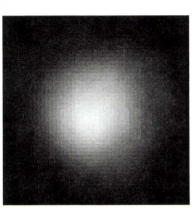

Fig. 2. Output beam spatial structure of 1.06 μm Nd:YAG laser radiation (2D image, Electrim CCD camera EDC-1000HR).

The coupling was realized by an achromatic doublet with a focal length 75 mm. The beam profile was checked behind the focusing optic, and it wasn't changed. The beam diameter in focus plane was measured 32 μm. The investigated waveguides were placed into the protector fixed in the adjustable holder. The energy delivery characteristics summary is in Table 1. The output beam structures behind the waveguides are shown in Figure 3 for 100 μm, and in Figure 4 for 250 μm inner diameter waveguides.

Table 1 – Delivery characteristics of 1.06 μm Nd:YAG laser radiation.

Number of waveguide (inner diameter)	Input energy	Output energy	Transmission
1A6-11-2 (100 μm)	0.49 mJ	0.47 mJ	95.8 %
C25-3-0 (250 μm)	0.68 mJ	0.46 mJ	67.1 %
C25-3-1 (250 μm)	0.68 mJ	0.55 mJ	80.8 %
C25-3-2 (250 μm)	0.68 mJ	0.52 mJ	76.6 %
C25-3-4 (250 μm)	0.68 mJ	0.51 mJ	74.3 %

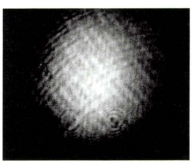

Fig. 3. Output beam spatial structure of 1.06 μm Nd:YAG laser radiation behind waveguide with 100 μm inner diameter and 10 cm length (2D image, Electrim CCD camera EDC-1000HR).

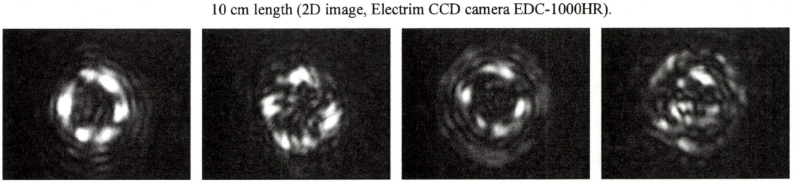

Fig. 4. Output beam spatial structure of 1.06 μm Nd:YAG laser radiation behind waveguides (C25-3-0, C25-3-1, C25-3-2, C25-3-4) with 250 μm inner diameter and 10 cm length (2D image, Electrim CCD camera EDC-1000HR).

3.2 Delivery of 1.34 μm Nd:YAG/V:YAG laser radiation

The output from the diode pumped Nd:YAG/V:YAG laser was fundamental TEM_{00} mode with $M^2 \cong 1$ (Fig. 5). The laser radiation output mean power was 25 mW. The measured pulse length was 6 ns, the corresponding pulse energy and peak power were 0.1 mJ and 16.7 kW, respectively

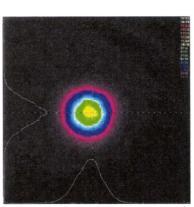

Fig. 5. Output beam spatial structure of 1.34 μm Nd:YAG/V:YAG laser radiation (2D and 3D image - pyroelectric camera Spiricon Pyrocam III).

The delivery measurement was analogous with the previous 1.06 μm Nd:YAG laser case; for coupling the plan-convex lens with focal length 75 mm was used. The energy delivery characteristics are shown in Table 2, as well as the output beam profiles are in Figure 6 and in Figure 7.

Table 2 – Delivery characteristics of 1.34 μm Nd:YAG/V:YAG laser radiation.

Number of waveguide (inner diameter)	Input mean power	Output mean power	Transmission
1A6-11-2 (100 μm)	14 mW	3.5 mW	25.0 %
C25-3-0 (250 μm)	22 mW	12.5 mW	56.8 %
C25-3-1 (250 μm)	22 mW	9.0 mW	40.9 %
C25-3-2 (250 μm)	22 mW	13.0 mW	59.1 %
C25-3-4 (250 μm)	22 mW	13.0 mW	59.1 %

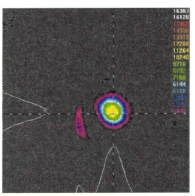

Fig. 6. Output beam spatial structure of 1.34 μm Nd:YAG laser radiation behind waveguide with 100 μm inner diameter and 10 cm length (2D and 3D image - pyroelectric camera Spiricon Pyrocam III).

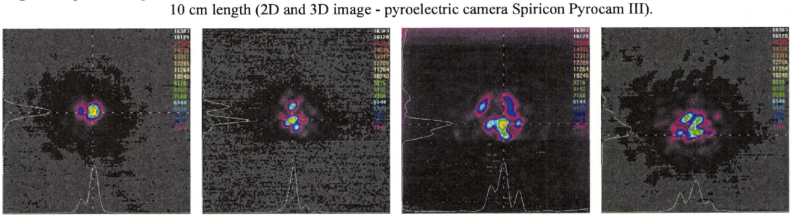

Fig. 7. Output beam spatial structure of 1.34 μm Nd:YAG laser radiation behind waveguide with 250 μm inner diameter and 10 cm length (2D and 3D image - pyroelectric camera Spiricon Pyrocam III).

4. DISCUSSION AND CONCLUSION

In this work, two Nd:YAG laser systems were designed and constructed. The both systems work in Q-switching regime and generated fundamental TEM_{00} mode. The first, Nd:YAG laser passively Q-switched by LiF:F^{2-} saturable absorber was pumped by Alexandrite laser radiation (755 nm, repetition rate 5 Hz) and generated radiation at 1.06 μm wavelength. The maximum output energy (power) and pulse length were 0.7 mJ (116.7 kW) and 6 ns, respectively. The second system was Nd:YAG/V:YAG microchip laser pumped by laser diode and generating the radiation at 1.34 μm wavelength. The output mean power, pulse length, and repetition rate were 25 mW, 6 ns, and 250 Hz, respectively. Corresponding pulse energy and peak power were 0.1 mJ and 16.7 kW, respectively.

As the major goal of this work, the delivery of high power near-infrared radiation (1.06 μm and 1.34 μm wavelength) by 100/190 μm and 250/360 μm thin hollow glass waveguides, and the modification of the beam spatial profile were investigated.

The summary of the energy transmission by the investigated waveguides is in Table 3. The decrease of value transmission on 25 % for wavelength 1.34 μm and 100 μm inner diameter waveguide was probably caused by damage of waveguide inner layers. So the check with another same type of this waveguide is necessary. Nevertheless the complete delivered transmission was more than 55 % and it can be sufficient for some application.

Table 3 - Transmission of radiations by investigated COP/Ag hollow glass waveguides.

Inner diameter	250 μm				100 μm
Number of waveguide	C25-3-0	C25-3-1	C25-3-2	C25-3-4	1A6-11-2
1.06 μm radiation	67.1 %	80.8 %	76.6 %	74.3 %	95.8 %
1.34 μm radiation	56.8 %	40.9 %	59.1 %	59.1 %	25.0 %

The delivered beam spatial structures for waveguides with corresponding inner diameters (100 μm and 250 μm) were similar for both investigated wavelength. From our results it follows that the spatial structure for 100 μm inner diameter waveguide is without significant changes (Fig.2 and Fig.3, Fig.5 and Fig.6).

The 250 μm inner diameter COP/Ag hollow glass waveguides do not keep the input beam fundamental profile. The differences of the input and output structures are shown in Fig.2 and Fig.4, and Fig.5 and Fig.7, for the case of 1.06 μm and 1.34 μm delivered laser radiation, respectively. The fundamental mode was changed into more peaks. The output beam spatial structure was rotated during fine angle adjustment of the waveguide input near the position with the maximum energy delivery.

The following measurement of the output beam structures is going to focus to the longer thin waveguides and to the modification of the delivery properties in the case of waveguide bending. The crucially important parameter will be the radiation losses for bent thin waveguides.

As summarization it can be concluded that the investigated delivery system with 100 μm inner diameter hollow glass waveguide appears as useful for the applications where the defined laser beam structure is required, for example the medical treatment (ophthalmology, microsurgery).

ACKNOWLEDGEMENT

This research has been supported by the Center for Advanced Telecommunications Technology Research Foundations (SCAT) and by grant JSPS No. 17206033, as well as by the Grant of the Czech Ministry of Education No.MSM6840770022 "Laser systems, radiation and modern optical applications".

REFERENCE

1. T. Dostálová, H. Jelínková, M. Miyagi, K. Hamal, and O. Krejsa, "Contact and non-contact laser preparation of hard dental tissues by Er:YAG laser radiation delivered by hollow glass waveguide or articulated arm", in Lasers in Dentistry, Proceedings of SPIE *3593*, 221-217, SPIE, (Washington), 1999.
2. M.Nakazawa, Y. Shi, K. Iwai, Y. Matsuura, X. Zhu, M. Miyagi, "Flexible hollow polycarbonate fiber for endoscopic infrared laser treatment", In: Novel Optical Instrumentation for Biomedical Applications III, Proceedings of SPIE Vol.*6631*, 66311A, 2007.
3. B. Dekel, Z. Barkay and A. Katzir, "The study of waveguides made by diffusion of Br into AgCl substrates and the transmission of mid-IR radiation through these waveguides", Optics Communications, Vol.199 (5-6), 383-388, 2001.
4. David J. Haan; James A. Harrington, "Hollow waveguides for gas sensing and near-IR applications", In: Specialty Fiber Optics for Medical Applications, Proceedings of SPIE Vol.*6596*, 43-49, 1999.
5. M.Němec, H.Jelínková, M.Fibrich, P.Koranda, M.Miyagi, K.Iwai, Yi-Wei Shi, Y.Matsuura, "Modification of mid-infrared radiation spatial structure caused by COP/Ag hollow waveguide", In: Optical Fibers and Sensors for Medical Diagnostics and Treatment Applications VII, Proceedings of SPIE Vol.*6433*, p. 643306, 2007.
6 J. Šulc, H. Jelínková, K. Nejezchleb, and V. Škoda, "Nd:YAG/V:YAG microchip laser operating at 1338 nm", Laser Physics Letters 2(11), pp. 519-524, 2005.